

Solving the Traveling Salesman Problem via Different Quantum Computing Architectures

Venkat Padmasola

Department of Physics

Center of Quantum Science and Engineering

Stevens Institute of Technology

Hoboken, N.J., 07030

vpadmaso@stevens.edu

Zhaotong Li

Department of Physics

Center of Quantum Science and Engineering

Stevens Institute of Technology

Hoboken, N.J., 07030

Zhli@stevens.edu

Rupak Chatterjee

Department of Applied Physics

Tandon School of Engineering

New York University

Brooklyn, NY 11201

Rupak.Chatterjee@NYU.edu

Wesley Dyk

Quantum Computing Inc.

215 Depot Court SE, Suite 215, Leesburg, VA 20175

wdyk@quantumcomputinginc.com

Abstract—We study the application of emerging photonic and quantum computing architectures to solving the Traveling Salesman Problem (TSP), a well-known NP-hard optimization problem. We investigate several approaches: Simulated Annealing (SA), Quadratic Unconstrained Binary Optimization (QUBO-Ising) methods implemented on quantum annealers and Optical Coherent Ising Machines, as well as the Quantum Approximate Optimization Algorithm (QAOA) and the Quantum Phase Estimation (QPE) algorithm on gate-based quantum computers.

QAOA and QPE were tested on the IBM Quantum platform. The QUBO-Ising method was explored using the D-Wave quantum annealer, which operates on superconducting Josephson junctions, and the Quantum Computing Inc (QCi) Dirac-1 entropy quantum optimization machine. Gate-based quantum computers demonstrated accurate results for small TSP instances in simulation. However, real quantum devices are hindered by noise and limited scalability. Circuit complexity grows with problem size, restricting performance to TSP instances with a maximum of 6 nodes.

In contrast, Ising-based architectures show improved scalability for larger problem sizes. SQUID-based Ising machines can handle TSP instances with up to 12 nodes, while entropy computing implemented in hybrid optoelectronic components extend this capability to 18 nodes. Nevertheless, the solutions tend to be suboptimal due to hardware limitations and challenges in achieving ground state convergence as the problem size increases. Despite these limitations, Ising machines demonstrate significant time advantages over classical methods, making them a promising candidate for solving larger-scale TSPs efficiently.

I. INTRODUCTION

The Traveling Salesman Problem (TSP) is an NP-hard optimization problem with a wide range of real-world applications, from optimizing delivery routes in supply chains to DNA sequencing [11]. The primary objective of the TSP is to determine a path starting from a given location, visiting every location in a specified list exactly once, and returning to the starting point while minimizing the total distance traveled. This problem involves strict, non-violable constraints, making it challenging to solve efficiently.

While the TSP is conceptually simple and can be solved for small graphs with well-defined edge connectivity, it becomes computationally intractable as the problem size increases. Table I shows the rapid growth in the number of possible paths as the number of nodes increases, highlighting the NP-hard nature of the problem.

Number of Nodes	Number of Possible Paths
5	12
10	181,000
20	6.1×10^{16}
25	3.1×10^{23}

TABLE I
GROWTH IN PROBLEM SIZE VERSUS NUMBER OF POSSIBLE PATH COMBINATIONS FOR THE TSP.

Significant efforts have been dedicated to the development of efficient algorithms to solve the TSP, given its diverse and impactful applications [12], [13]. In this paper, we leverage recent advances in computing hardware to explore novel approaches to solving the TSP. Specifically, we focus on quantum simulations, optical/optoelectronic computing, and quantum computing techniques to address the computational challenges posed by this problem.

II. THE TSP FORMULATION FOR GATE BASED QUANTUM COMPUTING

A. QAOA Formulation

1) *Theoretical formulation for the QAOA*: The quantum approximate optimization algorithm is a hybrid quantum-classical variational algorithm designed to tackle combinatorial optimization problems. An essential ingredient for understanding and deploying the QAOA is a constructive approach to carry out the outer-loop classical optimization. The performance of the QAOA on MaxCut problems has revealed its ability to exploit non-adiabatic operations [2]. For instance, the QAOA method compared to quantum annealing can succeed especially in scenarios adiabatic quantum

annealing fail due to a small spectral gap between the ground state and excited states. The comparison reveals that the QAOA can learn via optimization to utilize nonadiabatic mechanisms to circumvent the challenges associated with vanishing spectral gaps [2]. Finally, we provide a realistic resource analysis on the experimental implementation of the QAOA. When quantum fluctuations in measurements are accounted for, we illustrate that optimization is important only for problem sizes beyond numerical simulations but accessible on near-term devices.

For combinatorial optimization, the quantum approximate optimization algorithm briefly had a better approximation ratio than any known polynomial time classical algorithm until a more effective classical algorithm was proposed. The relative speed-up of the quantum algorithm is an open research question.

The heart of QAOA relies on the use of unitary operators dependent on $2p$ angles, where $p > 1$ is an input integer. These operators are iteratively applied on a state that is an equal weighted quantum superposition of all the possible states in the computational basis. In each iteration, the state is measured in the computational basis and the cost function f_Q is calculated. After a sufficient number of repetitions, the value of f_Q is almost optimal, and the state being measured is close to being optimal as well.

It was also shown that QAOA exhibits a strong dependence on the ratio of a problem's constraint to variables (problem density) [17] placing a limiting restriction on the algorithm's capacity to minimize a corresponding objective function.

It was soon recognized that a generalization of the QAOA process is essentially an alternating application of a continuous-time quantum walk on an underlying graph followed by a quality-dependent phase shift applied to each solution state. This generalized QAOA was termed the QWOA (Quantum Walk-Based Optimization Algorithm) [18].

In the paper [3] the authors conclude that a QAOA circuit with 420 qubits and 500 constraints would require at least one century to be simulated using a classical simulation algorithm running on state-of-the-art supercomputers so that would be sufficient for quantum computational supremacy.

To demonstrate solutions to the TSP using Universal gate based processors, we have explored known formulations of the QAOA, some of which are discussed below with specific processors as the quantum back-ends. Most known ways to formulate the TSP rely on defining the problem as a QUBO problem and then converting to a QAOA [30].

For a given classical "cost" function $f_C(x) : \mathbb{B}^n \rightarrow \mathbb{R}$, an approximate algorithm (for maximization) attempts to find a string x that achieves a desired approximation ratio r ,

$$\frac{f_C(x)}{f_C^{max}} \geq r \quad (1)$$

where f_C^{max} is the true maximum.

Consider the operator

$$\hat{H}_C = f_C(\sigma_z^1, \sigma_z^2, \dots, \sigma_z^N) \quad (2)$$

and the Hadamard basis

$$\begin{aligned} \mathbf{H}|0\rangle &= |+\rangle = \frac{|0\rangle + |1\rangle}{\sqrt{2}} = \frac{1}{\sqrt{2}} \begin{bmatrix} 1 \\ 1 \end{bmatrix} \\ \mathbf{H}|1\rangle &= |-\rangle = \frac{|0\rangle - |1\rangle}{\sqrt{2}} = \frac{1}{\sqrt{2}} \begin{bmatrix} 1 \\ -1 \end{bmatrix}. \end{aligned} \quad (3)$$

Consider an equally weighted superposition of all 2^n computational basis states by applying a direct product of Hadamard operators to $|0\rangle$,

$$\mathbf{H}^{\otimes n} |0\rangle = \frac{1}{\sqrt{2^n}} \sum_{z=0}^{2^n-1} |z\rangle \quad (4)$$

where $|z\rangle = |z_{n-1}z_{n-2}z_{n-3} \dots z_2z_1z_0\rangle$ represents the bit string corresponding to any integer as $z = 2^0z_0 + 2^1z_1 + \dots + 2^{n-1}z_{n-1}$. Each basis state is a eigenvector of \hat{H}_C

$$\hat{H}_C |z\rangle = f_C(\sigma_z^1, \sigma_z^2, \dots, \sigma_z^N) |z\rangle = f_C(z) |z\rangle \quad (5)$$

Let the maximum value f_C^{max} , being the largest eigenvalue of \hat{H}_C , correspond to the eigenvector $|z_{max}\rangle$ such that

$$\langle z_{max} | \hat{H}_C | z_{max} \rangle = f_C^{max} \quad (6)$$

One cannot in general find the state $|z_{max}\rangle$ but one can search for a state

$$|\psi\rangle = \sum_{z \in \{0,1\}^n} a_z |z\rangle \quad (7)$$

which is close as possible to $|z_{max}\rangle$.

2) The QAOA algorithm step sequence:

- 1) **Prepare the Initial State:** Begin with a uniform superposition of all possible computational basis states. For a system of n qubits, this state is prepared using Hadamard gates applied to each qubit:

$$|\psi_0\rangle = \mathbf{H}^{\otimes n} |0\rangle = \frac{1}{\sqrt{2^n}} \sum_{z=0}^{2^n-1} |z\rangle \quad (8)$$

- 2) **Construct the Problem Hamiltonian:** Define a Hamiltonian H_C that encodes the optimization problem's objective function. For example, if the goal is to minimize a cost function $C(z)$, then:

$$\hat{H}_C |z\rangle = f_C(\sigma_z^1, \sigma_z^2, \dots, \sigma_z^N) |z\rangle = f_C(z) |z\rangle \quad (9)$$

where $f_C(z)$ is the cost associated with the computational basis state $|z\rangle$.

- 3) **Construct the Mixer Hamiltonian:** Define a mixer Hamiltonian H_B that facilitates transitions between basis states. The typical choice is:

$$\hat{H}_B = \sum_{i=1}^n X_i, \quad (10)$$

where X_i is the Pauli-X operator acting on the i -th qubit. This Hamiltonian helps explore the solution space by driving transitions between states.

- 4) **Exponentiate and Parameterize:** Apply the problem Hamiltonian and mixer Hamiltonian alternately in p layers (referred to as the ' p -level' algorithm). Each layer is parameterized by angles γ and β , which control the evolution times. The resulting state after p steps is:

$$|\psi_p(\vec{\gamma}, \vec{\beta})\rangle = \prod_{j=1}^p e^{-i\beta_j \hat{H}_B} e^{-i\gamma_j \hat{H}_C} |\psi_0\rangle. \quad (11)$$

- 5) **Optimize Parameters:** Use a classical optimization algorithm to adjust the $2p$ parameters $\vec{\gamma} = (\gamma_1, \dots, \gamma_p)$ and $\vec{\beta} = (\beta_1, \dots, \beta_p)$ to maximize the expectation value of the problem Hamiltonian:

$$\langle H_C \rangle = \langle \psi_p(\vec{\gamma}, \vec{\beta}) | H_C | \psi_p(\vec{\gamma}, \vec{\beta}) \rangle. \quad (12)$$

The classical optimizer iteratively improves these parameters to find the optimal solution.

3) *Simulation Results on the IBMQ Platform for the QAOA Algorithm:* We initialize an arbitrary set of angles between 0 and 2π , which are passed through a classical COBYLA optimizer to determine the optimal set of angles. For a 4-node TSP, a 16-qubit circuit is initialized, as the qubit requirement scales as N^2 . The values pass through a quantum circuit with a depth of 6 layers. Therefore, there are 96 angles serving as hyperparameters for optimization. The output is then measured. Figure 1 illustrates a single layer of the six-layer QAOA quantum circuit, where the hyperparameters are encoded into the R_Y rotation gates.

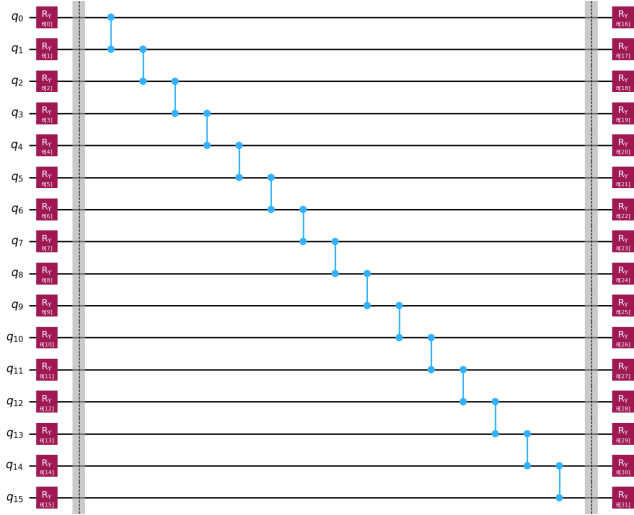


Fig. 1. A single layer of the six-layer QAOA quantum circuit.

The bar plots for the 96 angles before and after optimization are presented in Figures 2 and 3, respectively.

Figure 4 shows the convergence to the minimum cost during the optimization process using the QAOA approach.

For a Hamiltonian of size 16×16 , there are 2^{16} basis states. The measurement outcomes clearly demonstrate the need for an optimized set of angles for the R_Y rotation gates. A classical optimization step is required to fine-tune these

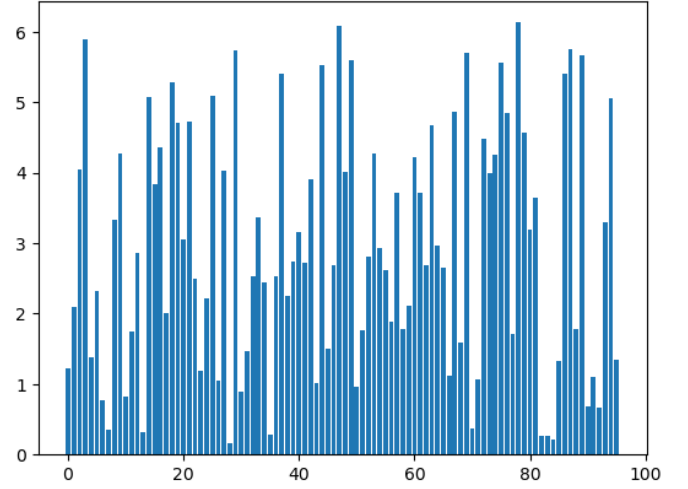


Fig. 2. Initial set of angles before optimization.

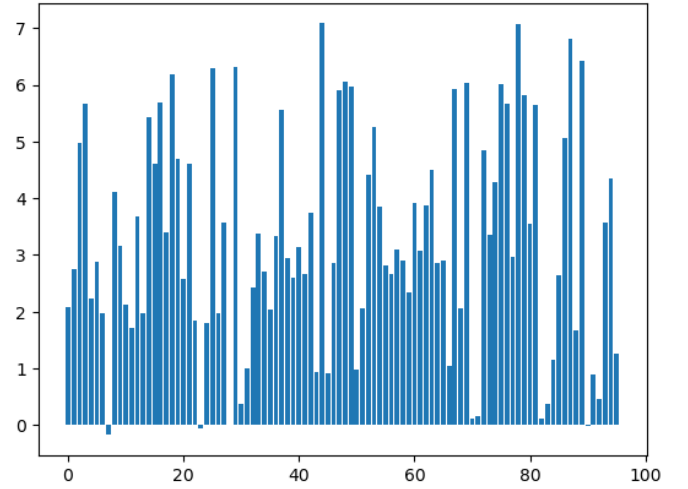


Fig. 3. Final set of angles obtained after optimization.

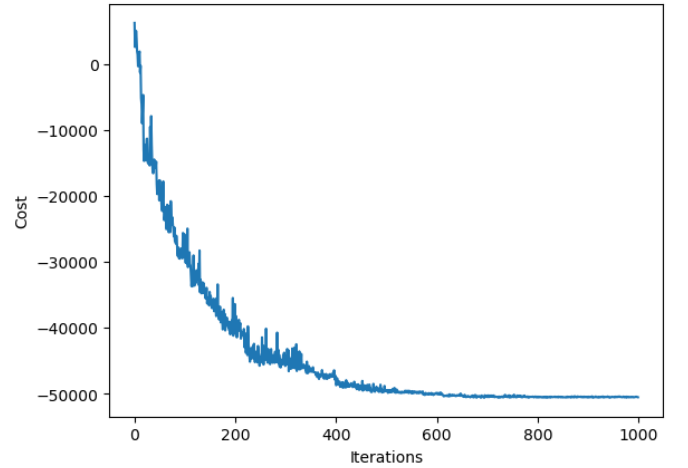


Fig. 4. Convergence to the optimal set of angles to determine the ground state of the QAOA Hamiltonian.

angles such that the Hamiltonian returns the correct solution with maximum probability. Fine-tuning the R_Y angle values is absolutely essential to ensure accurate solutions. Without this optimization, the results may violate constraints and yield incorrect solutions.

This observation highlights a significant limitation of the QAOA approach: the classical optimization step introduces a time bottleneck. As a result, QAOA cannot ensure polynomial time complexity due to the reliance on classical hyperparameter optimization.

B. The QPE Formulation

1) *Overview of the Quantum Phase Estimation Algorithm:* The Quantum Phase Estimation (QPE) algorithm extracts the phase θ associated with an eigenvalue of a unitary operator U [10]. Specifically, if $U|\psi\rangle = e^{2\pi i\theta}|\psi\rangle$, QPE estimates the phase θ with n -bit precision. The QPE circuit operates on two registers: the **upper register** of n qubits, initialized in $|0\rangle^{\otimes n}$, is used for phase estimation, and the **lower register** is initialized in the eigenstate $|\psi\rangle$ of U , such that $U|\psi\rangle = e^{2\pi i\theta}|\psi\rangle$. The key steps of QPE are as follows:

1) Apply Hadamard gates on all qubits of the upper register to create a superposition state.

2) Apply controlled- U^{2^j} operations, where j corresponds to each qubit in the upper register.

3) Apply the inverse Quantum Fourier Transform (QFT) on the upper register to extract the phase θ . The final state of the upper register encodes the binary representation of θ .

2) *Constructing the Unitary Operator U :* The unitary matrix U operates on a Hilbert space of dimension 2^m , where m is the number of qubits in the lower register. The action of U on an eigenstate $|\psi\rangle$ is:

$$U|\psi\rangle = e^{2\pi i\theta}|\psi\rangle. \quad (13)$$

The QPE algorithm requires the controlled- U operator, defined as:

$$C-U = |0\rangle\langle 0| \otimes I + |1\rangle\langle 1| \otimes U. \quad (14)$$

Here, $|0\rangle$ and $|1\rangle$ correspond to the control qubit states, and I is the identity matrix. The controlled- U^{2^j} operator generalizes this to:

$$C-U^{2^j} = |0\rangle\langle 0| \otimes I + |1\rangle\langle 1| \otimes U^{2^j}. \quad (15)$$

3) *Phase Kickback and Superposition State:* The Hadamard gate applied to the n -qubit upper register produces a superposition state:

$$|0\rangle^{\otimes n} \xrightarrow{H^{\otimes n}} \frac{1}{2^{n/2}} \sum_{k=0}^{2^n-1} |k\rangle, \quad (16)$$

where $|k\rangle$ represents the computational basis states. The controlled- U^{2^j} gates apply phase shifts based on the eigenvalue $e^{2\pi i\theta}$. For the j -th control qubit, the operation introduces a phase factor $e^{2\pi i \cdot 2^j \theta}$, resulting in the following state:

$$\frac{1}{2^{n/2}} \sum_{k=0}^{2^n-1} |k\rangle \otimes U^k |\psi\rangle. \quad (17)$$

By leveraging the eigenvalue relationship $U|\psi\rangle = e^{2\pi i\theta}|\psi\rangle$, the lower register accumulates phase factors:

$$\frac{1}{2^{n/2}} \sum_{k=0}^{2^n-1} e^{2\pi i k \theta} |k\rangle \otimes |\psi\rangle. \quad (18)$$

The upper register now contains the phase information encoded in the amplitudes of the basis states $|k\rangle$.

4) *Applying the Inverse QFT:* To extract the phase θ , we apply the inverse Quantum Fourier Transform (QFT) on the upper register. The QFT maps the amplitudes $e^{2\pi i k \theta}$ into the binary representation of θ with high probability. The inverse QFT is defined as:

$$\text{QFT}^\dagger |k\rangle = \frac{1}{2^{n/2}} \sum_{j=0}^{2^n-1} e^{-2\pi i k j / 2^n} |j\rangle. \quad (19)$$

After applying QFT^\dagger , the upper register collapses to a computational basis state $|j\rangle$, where j represents the binary approximation of $2^n \theta$. That is, the output of the QPE algorithm is the n -bit approximation of the phase θ , such that:

$$\theta \approx \frac{j}{2^n}, \quad j \in \{0, 1, \dots, 2^n - 1\}. \quad (20)$$

5) *Encoding Hamiltonian Cycles:* If QPE is applied to a system where the unitary U encodes Hamiltonian cycles as needed for the TSP problem, the eigenstates $|\psi\rangle$ are expressed as:

$$|\psi\rangle = \bigotimes_{j=1}^n |i(j) - 1\rangle_2, \quad (21)$$

where $i(j)$ represents the index of the city visited at step j . For example, for the sequence 1 – 2 – 4 – 3:

$$|i(1) - 1\rangle = |2\rangle = |10\rangle_2, \quad (22)$$

$$|i(2) - 1\rangle = |0\rangle = |00\rangle_2, \quad (23)$$

$$|i(4) - 1\rangle = |1\rangle = |01\rangle_2, \quad (24)$$

$$|i(3) - 1\rangle = |3\rangle = |11\rangle_2. \quad (25)$$

The complete encoded state is:

$$|\psi\rangle = |10\rangle \otimes |00\rangle \otimes |01\rangle \otimes |11\rangle = |10001111\rangle. \quad (26)$$

In its simplest form, the quantum phase estimation (QPE) circuit operates on two registers of qubits. The lower register is repeatedly acted on by a controlled- U operator, where the control qubits are in the upper register. An inverse quantum Fourier transform (QFT) is then applied to the upper register, which serves as the estimator for an n -bit estimate of the phase θ . Applying this circuit block to a 16-qubit case, we obtain the following quantum circuit. Figure 5 illustrates the basic setup for QPE.

To encode any arbitrary distance matrix to a format suitable for the QPE algorithm, we first normalize the values in raw distance matrix such that all the values are in between 0 and 1. We do this so that any such value can be represented by euler phase angles (the exponents are the phase angles which lie between 0 and 2π).

The matrix B is a representation of the normalized distance matrix encodes as euler phases.

$$B = \begin{bmatrix} e^{i\phi_{1 \rightarrow 1}} & e^{i\phi_{1 \rightarrow 2}} & e^{i\phi_{1 \rightarrow 3}} & e^{i\phi_{1 \rightarrow 4}} \\ e^{i\phi_{2 \rightarrow 1}} & e^{i\phi_{2 \rightarrow 2}} & e^{i\phi_{2 \rightarrow 3}} & e^{i\phi_{2 \rightarrow 4}} \\ e^{i\phi_{3 \rightarrow 1}} & e^{i\phi_{3 \rightarrow 2}} & e^{i\phi_{3 \rightarrow 3}} & e^{i\phi_{3 \rightarrow 4}} \\ e^{i\phi_{4 \rightarrow 1}} & e^{i\phi_{4 \rightarrow 2}} & e^{i\phi_{4 \rightarrow 3}} & e^{i\phi_{4 \rightarrow 4}} \end{bmatrix} \quad (27)$$

Since we have a 4 node distance matrix, we then construct 4 unitary operators U_j from B such that $(U_j)_{k,k} = [B]_{j,k}$:

$$U_j = \text{diag}(B_{j,1}, B_{j,2}, B_{j,3}, B_{j,4}) \quad (28)$$

Finally, the tensor product of the 4 U_j operators $U = U_1 \otimes U_2 \otimes U_3 \otimes U_4$ will also be a unitary matrix.

We define U_j generally as

$$U_j = \left(\sum_{k=1}^n B[j][k] \times \text{outer product of basis vectors} \right) \quad (29)$$

That is,

$$U_1 = \begin{bmatrix} e^{i\phi_{1 \rightarrow 1}} & 0 & 0 & 0 \\ 0 & e^{i\phi_{2 \rightarrow 1}} & 0 & 0 \\ 0 & 0 & e^{i\phi_{3 \rightarrow 1}} & 0 \\ 0 & 0 & 0 & e^{i\phi_{4 \rightarrow 1}} \end{bmatrix}$$

$$U_2 = \begin{bmatrix} e^{i\phi_{1 \rightarrow 2}} & 0 & 0 & 0 \\ 0 & e^{i\phi_{2 \rightarrow 2}} & 0 & 0 \\ 0 & 0 & e^{i\phi_{3 \rightarrow 2}} & 0 \\ 0 & 0 & 0 & e^{i\phi_{4 \rightarrow 2}} \end{bmatrix}$$

$$U_3 = \begin{bmatrix} e^{i\phi_{1 \rightarrow 3}} & 0 & 0 & 0 \\ 0 & e^{i\phi_{2 \rightarrow 3}} & 0 & 0 \\ 0 & 0 & e^{i\phi_{3 \rightarrow 3}} & 0 \\ 0 & 0 & 0 & e^{i\phi_{4 \rightarrow 3}} \end{bmatrix}$$

$$U_4 = \begin{bmatrix} e^{i\phi_{1 \rightarrow 4}} & 0 & 0 & 0 \\ 0 & e^{i\phi_{2 \rightarrow 4}} & 0 & 0 \\ 0 & 0 & e^{i\phi_{3 \rightarrow 4}} & 0 \\ 0 & 0 & 0 & e^{i\phi_{4 \rightarrow 4}} \end{bmatrix}$$

Creating the final unitary matrix U from the series of submatrices U_i The way U defined is:

$$U = U_1 \otimes U_2 \otimes U_3 \otimes U_4$$

6) *Simulation and experimental results for the QPE algorithm on IBMQ platform:* The QPE method has certain advantages over the QAOA approach significantly due to the fact that for a problem of size n , the qubit requirement in the case of QPE being $n \log n$ as opposed to the n^2 qubit requirement in the case of QAOA.

It is evident that real quantum computers are prone to errors due to noise, as illustrated in Figure 7, while the simulation results yield more accurate results, as shown in Figure 6. Previous studies have demonstrated that NISQ gate-based quantum computers are not yet sufficiently advanced for fault tolerance or large enough to achieve quantum advantage [23].

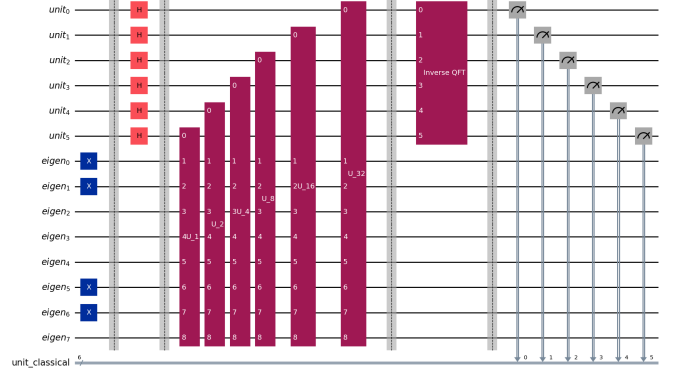


Fig. 5. Circuit for Quantum Phase Estimation(QPE)

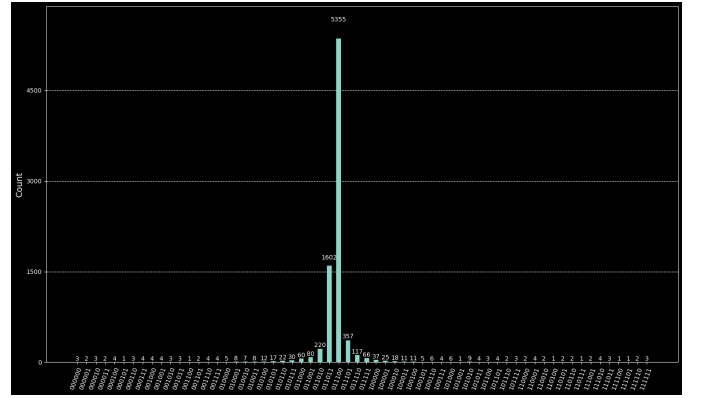


Fig. 6. Histogram of the measurement results for 8192 shots for the QPE using the IBM QASM simulator

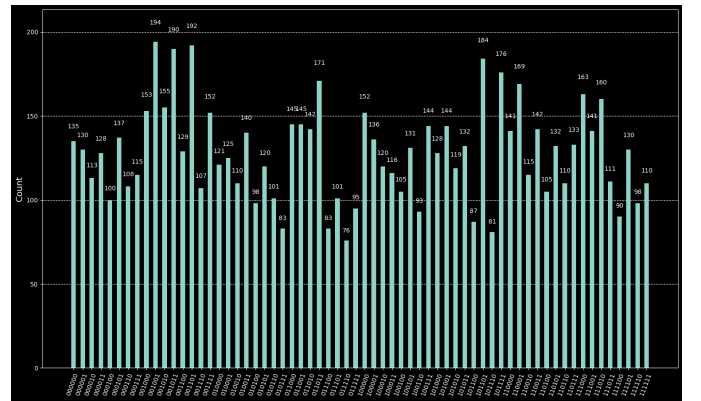


Fig. 7. Histogram of the measurement results for 8192 shots for the QPE using the IBM Brisbane Quantum Computer

To obtain reliable outputs from universal gate-based quantum computers in the NISQ era, quantum error correction or error mitigation techniques are essential [24]. Consequently, it is imperative to explore alternative computing architectures that can potentially provide polynomial-time advantages. In the following sections, we investigate alternative approaches to solving the TSP using Ising-type simulators and hardware.

III. THE TSP FORMULATION FOR ISING TYPE SIMULATORS AND HARDWARE

A. Ising and QUBO Models

The Ising model and its equivalent Quadratic Unconstrained Binary Optimization (QUBO) formulation constitute a central problem class for adiabatic quantum computation (AQC), where they are solved through a physical process known as quantum annealing.

In this model, we consider a set Λ of lattice sites, each with a set of adjacent sites forming a lattice or graph structure. For each lattice site $k \in \Lambda$, there is a discrete variable σ_k such that $\sigma_k \in +1, -1$, representing the spin states of a system. Any two adjacent sites, or “nearest neighbors,” $i, j \in \Lambda$ interact with an exchange coefficient J_{ij} . Additionally, each site $j \in \Lambda$ may experience an external magnetic field h_j . The energy of a spin configuration $\sigma = (\sigma_1, \sigma_2, \dots)$ is given by the following Hamiltonian:

$$H(\sigma) = - \sum_{\langle i, j \rangle} J_{ij} \sigma_i \sigma_j - \mu \sum_j h_j \sigma_j, \quad (30)$$

where μ represents the magnetic moment.

A specific spin configuration σ follows a probability distribution given by the Boltzmann distribution with inverse temperature $\beta \geq 0$:

$$P_\beta(\sigma) = \frac{e^{-\beta H(\sigma)}}{Z_\beta}, \quad (31)$$

where the partition function Z_β is defined as:

$$Z_\beta = \sum_{\sigma} e^{-\beta H(\sigma)}. \quad (32)$$

The expectation value of a function f over spin configurations is given by:

$$\langle f \rangle_\beta = \sum_{\sigma} f(\sigma) P_\beta(\sigma). \quad (33)$$

The QUBO model is an alternative formulation of the Ising model that replaces spin variables (± 1) with binary variables (0, 1). This model is widely used in combinatorial optimization, including applications in finance, machine learning, and logistics. The QUBO formulation is NP-hard and often serves as a bridge between classical and quantum approaches to optimization [5]. For many classical problems such as the maximum cut graph problem, embeddings into a QUBO formulation are well known [4]. Embeddings for machine learning models include support vector machines [32], clustering, and probabilistic graphical models [31]. An

almost equivalent physical model, the Ising model, has a well known QUBO formulation.

The transformation from the Ising model to QUBO is straightforward and is achieved using the following linear transformation:

$$x_i = \frac{1 + \sigma_i}{2}, \quad x_j = \frac{1 + \sigma_j}{2}. \quad (34)$$

This ensures that for any $\sigma_i, \sigma_j \in +1, -1$, we obtain binary variables $x_i, x_j \in 0, 1$.

Consider a quadratic function $f : \mathbb{B}^n \rightarrow \mathbb{R}$, defined over an n -dimensional binary space:

$$f_Q(x) = \sum_{i=1}^n \sum_{j=1}^i q_{ij} x_i x_j, \quad (35)$$

where $q_{ij} \in \mathbb{R}$, $1 \leq j \leq i \leq n$, and $x_i \in \mathbb{B} = 0, 1$. The goal of QUBO is to find an n -dimensional binary vector x that minimizes this function:

$$x = \arg \min_{x \in \mathbb{B}^n} f_Q(x). \quad (36)$$

The QUBO function f_Q can be rewritten using a symmetric QUBO matrix $Q \in \mathbb{R}^{n \times n}$, $Q = [q_{ij}]$:

$$f_Q(x) = x^\top Q x. \quad (37)$$

This matrix representation allows QUBO problems to be efficiently mapped onto quantum annealers or specialized quantum hardware for solving large-scale optimization problems.

B. The TSP Formulation for Simulated Annealing

Simulated Annealing (SA) is a classical optimization algorithm inspired by the annealing process in metallurgy, where a material is gradually cooled to remove defects and reach a stable low-energy state. SA applies this concept to optimization problems by slowly decreasing the system’s temperature, allowing it to explore the solution space and settle into a low-energy configuration. However, SA can be computationally expensive due to its reliance on sequential updates of spin states. Nonetheless, it provides a unique approach to solving the Traveling Salesman Problem (TSP) by leveraging principles that differ fundamentally from universal gate-based quantum machines.

Mathematically, SA closely resembles the formulation of an Ising-type quantum computer. It explores the entire solution space, enabling it to escape local optima. Unlike gradient-based methods, SA does not get trapped in suboptimal solutions since it incorporates randomness to explore neighboring states. This stochastic nature helps the algorithm bypass local minima. However, in highly complex landscapes with numerous local minima, especially for large problem sizes, SA may fail to reach the true ground state solution.

The annealing process involves gradually lowering the “temperature,” allowing the algorithm to initially explore a broad set of solutions, including suboptimal ones, before progressively converging toward an optimal or near-optimal

solution. This approach enables SA to handle complex, non-convex objective functions without requiring derivatives or assumptions about the function's structure. It performs effectively even in noisy or irregular problem spaces.

Despite its advantages, SA is not always the fastest or most precise optimization method. Depending on the problem, alternative approaches such as genetic algorithms, particle swarm optimization, or gradient-based techniques may yield better results. Additionally, selecting appropriate coefficients and tuning parameters for SA is critical, as improper settings can significantly affect its performance. A systematic strategy for parameter optimization is necessary to enhance the algorithm's efficiency and effectiveness in solving large-scale optimization problems.

1) *Hamiltonian formulation for Simulated Annealing:* One of the most straightforward ways to solve the TSP is to convert it into a Quadratic Unconstrained Binary Optimization (QUBO) problem. For an unconstrained TSP problem, we can use a binary variable a_{ik} to represent whether the city k is visited ($a_{ik} = 1$) or not ($a_{ik} = 0$) at the i -th step, shown in figure 8. The objective function can therefore be defined in a quadratic form:

$$H_{obj} = \sum_{k \neq l} \sum_i W_{kl} a_{ik} a_{(i+1)l} \quad (38)$$

Where W_{kl} is the element of the distance matrix for distance between city k and city l . Since each city should only be visited once, and only a single city can be visited simultaneously, we introduce the two constrains:

$$H_{cons} = \sum_i \left(\sum_k a_{ik} - 1 \right)^2 + \sum_k \left(\sum_i a_{ik} - 1 \right)^2 \quad (39)$$

If we replace $a_{ik} = (\sigma_{ik} + 1)/2$ where $\sigma_{ik} = \pm 1$ represents an Ising spin, the QUBO formulation is mathematically equivalent to an Ising Hamiltonian:

$$\begin{aligned} H &= H_{obj} + \gamma H_{cons} \\ &= \frac{1}{4} \sum_{k \neq l} \sum_i W_{kl} \sigma_{ik} \sigma_{(i+1)l} + \frac{1}{2} \sum_{k \neq l} \sum_i W_{kl} \sigma_{ik} \\ &\quad + \frac{\gamma}{4} \sum_i \sum_k \sum_l \sigma_{ik} \sigma_{il} + \frac{\gamma}{2} (n-2) \sum_i \sum_k \sigma_{ik} \\ &\quad + \frac{\gamma}{4} \sum_k \sum_i \sum_j \sigma_{ik} \sigma_{jk} + \frac{\gamma}{2} (n-2) \sum_k \sum_i \sigma_{ik} \\ &\quad + const. \end{aligned} \quad (40)$$

For a randomly generated distance matrix W , figure 9 shows the interaction matrix J reshaped into 2D when $\gamma = 5$.

To demonstrate how the Hamiltonian appears after the adjacency matrix transforms under the equations described above, a heat map of the Hamiltonian for a 6 city TSP is plotted as shown in figure 9.

2) *Solution for a 6 city TSP using Simulated Annealing:* The solution obtained from this Hamiltonian is initially represented as a linear array of 36 spins, which is then reshaped into a 6×6 square matrix encoding the solution path, ensuring that each row and column contains

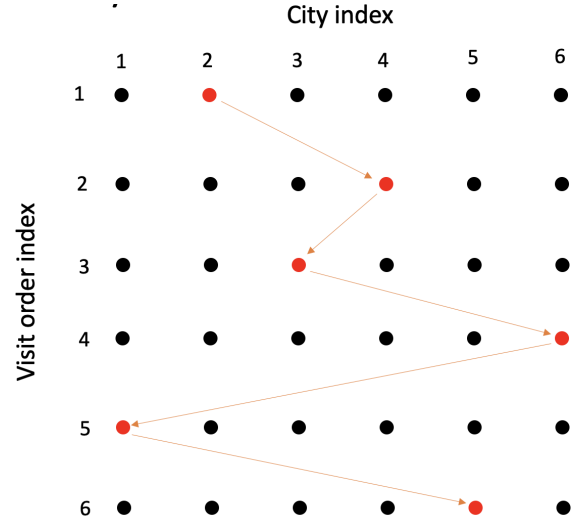


Fig. 8. routing for a TSP solution under QUBO formulation. The spins are arranged in two dimensions, where the x-axis represents the index of each city and the y-axis is the visitation order

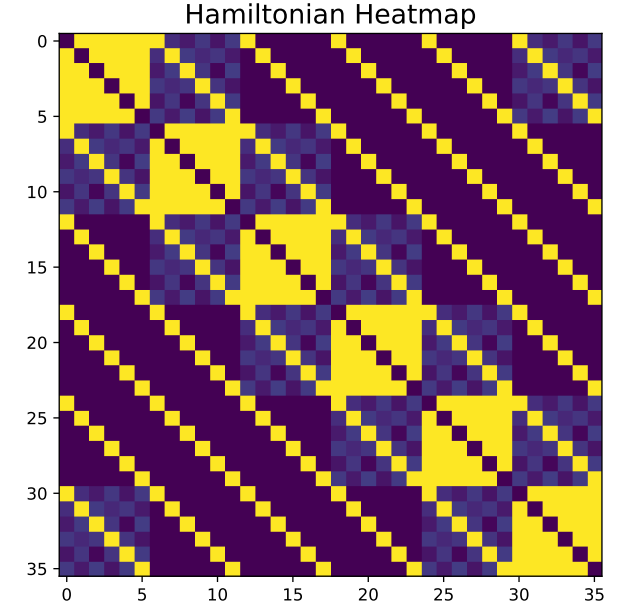


Fig. 9. Hamiltonian matrix for 6 cities

exactly one +1 spin value. Figure 10 illustrates the plot of Ising energy converging to the lowest value over the time steps, demonstrating the working mechanism of the simulated annealing algorithm. The final low-energy solution is visualized both as a heat map and a directed graph.

C. Experimental Observations for Adiabatic Quantum computers

1) *Hamiltonian formulation for the D-Wave platforms:* Consider N "cities" (vertices in a graph) indexed as $\{0, 1, \dots, N-1\}$. Consider the case of a round trip returning to the original city (Hamilton cycle). As each city maybe visited

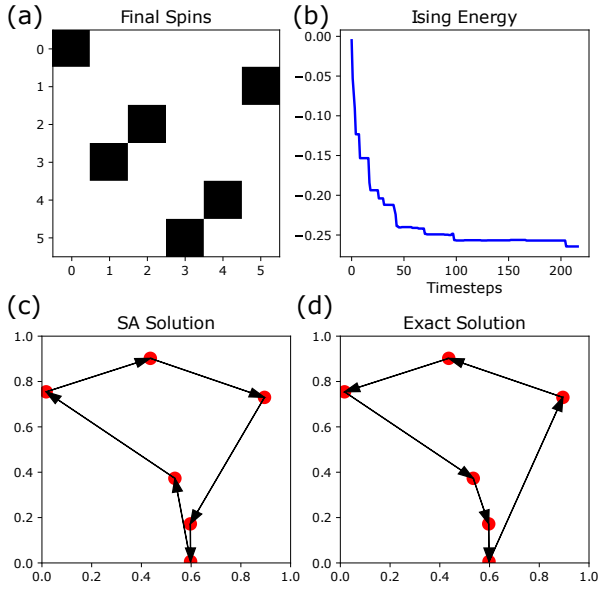


Fig. 10. Simulated annealing solution for a 6 city TSP. (a) The solution of a 6-city TSP by SA. (b) The Ising energy as a function of the number of time steps. (c) The directed graph of the solution obtained by SA. (d) The directed graph of the solution obtained by the brute force method.

only once, there will be N time steps indexed as $\{1, \dots, N\}$ where we start at $t = 0$. Consider $N + 1$ sets of $N + 1$ binary variables

$$x_{i,t} \in \mathbb{B}, \quad i \in \{0, 1, \dots, N\}, \quad t \in \{0, 1, \dots, N\} \quad (41)$$

$x_{i,t} = 1$ denotes that the i^{th} city was reached in the t^{th} time. Let us start at the 0^{th} city such that we have a boundary condition of $x_{0,0} = 1$. The last city visited at $t = N$ must be the original city, so we have another boundary condition $x_{N,N} = 1$ where city N is required to be equal to city 0 (recall that the unique cities are indexed as $\{0, 1, \dots, N - 1\}$).

Let d_{ij} denote a distance (directed graph edge) between the i^{th} and j^{th} cities. The tour length is given by

$$H_{\text{tour}} = \sum_{i,j=0}^N d_{ij} \sum_{t=0}^{N-1} x_{i,t} x_{j,t+1} \quad (42)$$

There exist two main constraints. First, one may travel to each city (vertex) only once. Consider the i^{th} city. If one looks at a whole time cycle summing over all times one needs

$$\sum_{t=0}^N x_{i,t} = 1, \quad \forall i \in \{0, 1, \dots, N\} \quad (43)$$

For instance, if the i^{th} city was never visited, this sum would be 0. If a city was visited more than once, this sum would be > 1 . Second, one must travel to every city once (each time step contains only one city) producing the condition that

$$\sum_{i=0}^N x_{i,t} = 1, \quad \forall t \in \{0, 1, \dots, N\} \quad (44)$$

Such a round trip tour is called a *Hamilton cycle*.

Both these constraints must be added to the tour Hamiltonian H_{tour} to give the TSP minimization function

$$\begin{aligned} H_{\text{TSP}} &= H_{\text{tour}} + \text{constraint terms} \\ &= \sum_{i,j=0}^N d_{ij} \sum_{t=0}^{N-1} x_{i,t} x_{j,t+1} + \lambda \sum_{i=0}^N \left(\sum_{t=0}^N x_{i,t} - 1 \right)^2 \\ &\quad + \lambda \sum_{t=0}^N \left(\sum_{i=0}^N x_{i,t} - 1 \right)^2 \end{aligned} \quad (45)$$

The ground state of this Hamiltonian is the solution of the TSP problem.

2) *Constraints*: For a problem of size N , there are $\binom{n}{2}$ constraints. The constraint matrices corresponding to these constraint terms must match the number of constraints [6]. In the AQC formulation of the problem, enforcing hard constraints presents a challenge, as introducing high penalty terms often eliminates the feasibility of solutions. Therefore, it is crucial to establish bounded values for the Lagrange parameter to obtain the most optimal solutions. Additionally, chain strength plays a significant role in determining the feasibility and quality of returned solutions, ensuring that constraints are not violated.

Although D-Wave processors continue to improve, enabling the embedding of larger graphs, the majority of returned solutions remain suboptimal. Further research is necessary to identify the key parameters that significantly influence solution quality. Refining these parameters could enhance the likelihood of achieving optimal solutions with the highest number of valid samples.

3) *Normalization*: Since the AQC formulation is sensitive to variations in the Lagrange parameter, making it challenging to enforce constraints effectively, additional steps are necessary to carefully select an appropriate Lagrange parameter. A plot of constraint violation probability is shown in Figure 11 for test graphs with random weights.

From recent efforts to enforce constraints rigorously before sampling energies and constructing solutions, we have observed that normalizing or scaling the matrix of weights significantly increases the likelihood of finding a feasible solution.

We conducted 10 test runs of the TSP code on each test graph for two cases: one without normalization and the other with normalization applied. As shown in Table II, normalizing the weight matrix enhances the probability of obtaining a feasible solution. Figure 12 compares the constraint violation probability for test graphs with random weights on the D-Wave Advantage6.1 machine, both with and without normalization.

4) *Hardware architecture*: The D-Wave platform provides quantum computing capabilities through its signature superconducting hardware, which leverages quantum tunneling across potential barriers to reach the ground state.

The D-Wave QPU consists primarily of nodes made from superconducting Josephson junctions that function as two-state

qubits, forming a binary system. These qubits are coupled using RF-SQUIDS [28]. At near-zero Kelvin temperatures, the system's possible energy states collapse to a singular value, corresponding to the lowest energy state or ground state. This principle, rooted in well-established thermodynamics, forms the fundamental operational mechanism of D-Wave hardware.

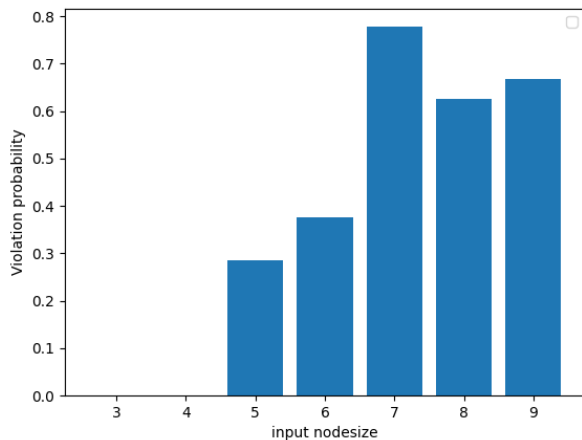


Fig. 11. Plot of Graph Size Vs. Violation Probability for random inputs.

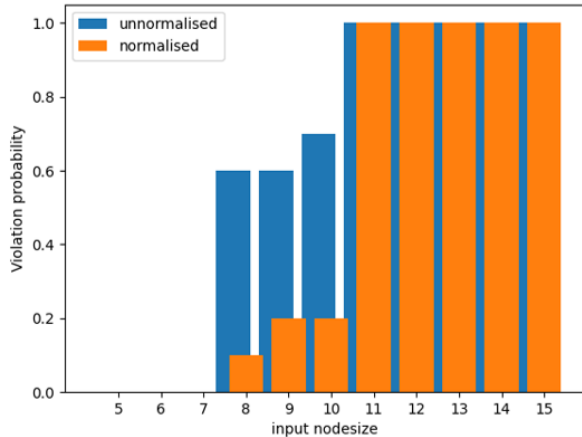


Fig. 12. Plot of Graph Size Vs. Violation Probability for selected test cases.

Graph-size	solutions without normalization	solutions with normalization
8	4	9
9	4	8
10	3	8

TABLE II

THE TABLE SHOWS THE NUMBER OF RUNS VS THE NUMBER OF FEASIBLE SOLUTIONS WITH AND WITHOUT NORMALIZATION.

5) *Solution for an 8 node TSP solved by the Dwave machines:* An 8 node graph and its solution is shown in figure 16

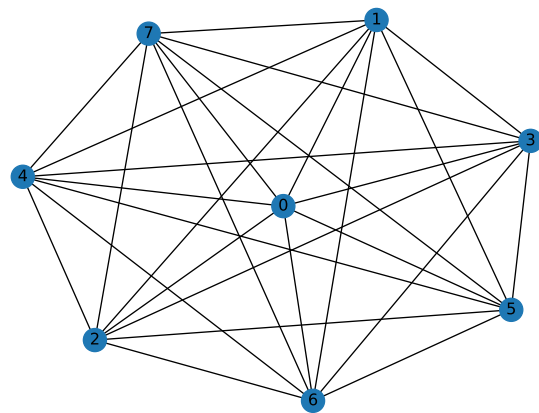


Fig. 13. 8 node input graph

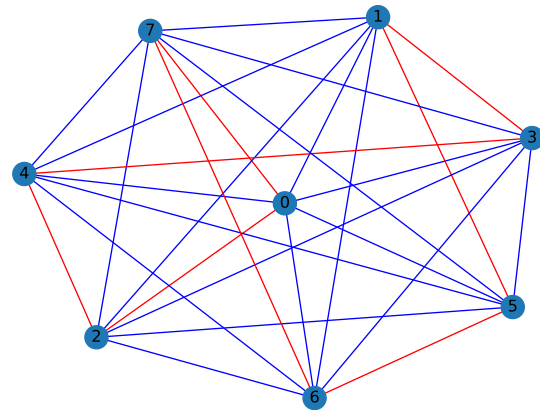


Fig. 14. 8 node output graph

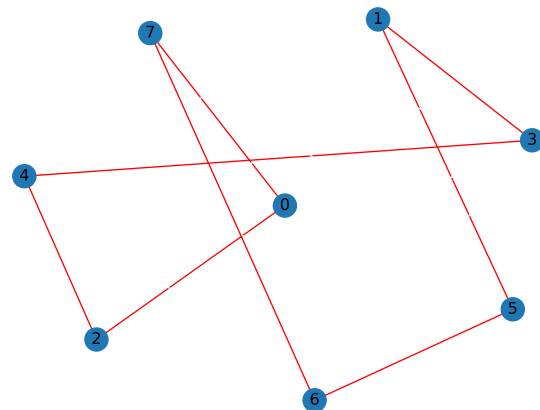


Fig. 15. 8 node output graph with the highlighted solution path

Fig. 16. The 8 node graph solved by D-wave quantum annealers. Plot (a) is the problem graph and plot (b) is the solution graph. Plot (c) is the highlighted solution path

D. Experimental Observations for Optical Ising computers

The large-scale optical Ising machine represents a significant advance in photonic computing. This system utilizes a spatial light modulator (SLM), a device that imposes spatially varying modulation on a beam of light. In this configuration, the spin variables of the Ising problem are encoded through binary phase modulation of the light field [7]. Essentially, the phase of the light field corresponding to the position of the wave at a given point in space is modified in a binary manner to represent the spin variables.

A key challenge facing optical Ising machines is the difficulty in encoding the coupling coefficients J_{ij} onto the SLM for a spatial optical Ising machine. One potential solution to this issue is the application of gauge transformations [25], which provides an alternative approach to improve the efficiency and accuracy of encoding.

1) *Hamiltonian formulation on the QCI Dirac platforms:* QCI is currently offering hybrid quantum optimization machines that can solve discrete and quasi-continuous variables (Dirac-3) or QUBO/Ising problems (Dirac-1) like D-wave quantum annealers. Dirac-3 has been shown to additionally solve integer linear programming models and mixed integer linear programming models with a solution space spanning a range of integers without explicitly converting such a problem to binary. This allows us to use ILP formulations directly without any conversions to define the TSP to be solved on the QCI platforms. Two most popular ILP formulations that are being tested here are the Miller–Tucker–Zemlin [26] formulation and the Dantzig–Fulkerson–Johnson formulation [27].

$$\min \sum_{i=1}^n \sum_{j=1}^n c_{ij} x_{ij} \quad (46)$$

where c_{ij} is the cost of traveling from city i to city j , and x_{ij} is a binary variable indicating whether the path from i to j is included in the tour.

2) *Subtour Elimination Constraints:* Introduce variables u_i to represent the order in which cities are visited:

$$u_j - u_i \geq 1 - (n-1)(1-x_{ij}) \quad \forall i, j \in \{2, \dots, n\}, i \neq j \quad (47)$$

These constraints ensure that no subtours are formed.

3) *Additional Constraints:* Each city must be visited exactly once:

$$\sum_{j=1}^n x_{ij} = 1 \quad \forall i \quad (48)$$

$$\sum_{i=1}^n x_{ij} = 1 \quad \forall j \quad (49)$$

The order variables must be within a valid range:

$$2 \leq u_i \leq n \quad \forall i \in \{2, \dots, n\} \quad (50)$$

4) *Hardware architecture:* Entropy quantum computing was recently introduced as an efficient optimization technique that leverages the principles of entropy minimization to guide quantum state evolution toward optimal solutions of a Hamiltonian [33]. In a photonic realization, qudits are encoded as a superposition of photon numbers in time bins that evolve in an optical fiber loop which embeds a desired Hamiltonian as a dissipative operator. This effectively emulates imaginary time evolution, in which the propagation of higher-energy eigenstates is subject to dissipation and decoherence while the lower-energy eigenstates are promoted in this evolution.

The current generation of the Entropy Quantum Computing (EQC) hardware at QCI, named Dirac-3, is a hybrid system that harnesses the high-speed parallel processing capabilities of photonics and the quantum nature of light with the precise control and programmability of electronic circuits. By leveraging photonic systems for entropy-driven state evolution—enabled by their natural ability to manipulate complex optical fields—and utilizing electronics for state initialization, feedback, and fine-tuning, hybrid entropy computing achieves efficient optimization. Such systems can explore large solution spaces rapidly through photonic modes propagation while employing electronic components to refine solutions iteratively. This synergy offers a pathway for solving challenging optimization problems in areas such as machine learning, signal processing, and network design, with the potential for high speed, low power consumption, and scalability.

The EQC hardware Dirac-1 targets optimization of a polynomial objective function E in the following form:

$$E = \sum_i C_i x_i + \sum_{i,j} J_{ij} x_i x_j. \quad (51)$$

where, $x_i \in \{0, 1\}$ are optimization variables, C_i are real-valued coefficients of linear terms, and J_{ij} represent two-body interaction coefficients that are real numbers subject to the tensor J being symmetric under all permutations of the indices. Governed by the physical mechanism of operation of the EQC hardware, x_i represents photon numbers in the i 'th time bin degrees of freedom.

A major advantage of EQC compared to other quantum annealers is its flexible variable encoding capability [33]. While, in the form discussed above, EQC allows for solving continuous-variable optimization problems, by allocating multiple photon time bins to one variable, one can effectively encode binary or integer variables for solving combinatorial optimization problems in the forms of binary, integer or even mixed-integer problems.

Researchers have shown that by doing this, the propagation of light can be tailored or adjusted to minimize an Ising Hamiltonian. Using Min-Max normalization to ensure a successful Hamilton cycle, the photonic Ising machine Can solve the TSP for a problem upto 18 nodes for any linear constraints of the type $Ax = b$.

With the advantage of all-to-all connectivity no explicit embedding step is required as opposed to the D-wave platform

[22], the QCI Dirac machines are able to solve TSP instances of sizes beyond 12 nodes.

5) *Solution for an 18 node TSP:* The maximum size of the TSP that can be solved reliably without violating the constraints is currently 18 nodes. Figures 20 is a demonstration of the Dirac-1 machine solving a TSP instance of 18 nodes.

IV. RESULTS

We can clearly see that the Traveling Salesman Problem (TSP) is well-suited for direct Ising-type processors, as the cost function is inherently quadratic, contrasting with the quantum algorithms that utilize universal gate-based quantum processors. With ongoing advancements in the design and functionality of Ising-type quantum machines, we have not only demonstrated proofs of concept for small test cases but also addressed the scalability challenges. These improvements bring us closer to developing robust practical applications for solving real-world optimization problems.

Although our results confirm that Ising-based processors can effectively solve the TSP [19], it remains crucial to verify whether the returned solutions are optimal. A common challenge with current Ising-based machines is their tendency to become trapped in local minima rather than converging to the global minimum [20]. A thorough assessment is required to compare the obtained solutions with classical counterparts to ensure that the identified Hamiltonian cycle is not only valid but also represents the true minimum weight configuration.

Verification against classical solutions reveals that Ising processors do not always return the ground state solution and often produce suboptimal results. However, for smaller problem instances, Ising machines exhibit higher accuracy in finding optimal solutions. To enhance the reliability of the results, multiple solution samples should be collected and statistically evaluated. The probability of obtaining the true ground state solution improves with an increasing number of sampled runs.

TSP Algorithm	Time Complexity
Brute Force	$O(n!n)$
Christofides algorithm	$O(n^3)$
Christofides with Serdyukov approximation	$O(n^3 \log n)$
Nearest Neighbour algorithm	$O(n^2)$
Dynamic Programming	$O(2^n * n^2)$
Simulated Annealing	$O(1.62^n * n^2)$
Ambiani's et. al.	$O(1.728^n)$
QUBO on Dwave (best case)	$O(2 \log n)$
QUBO on Dirac-1	$O(n^{3/2})$

TABLE III
TIME COMPLEXITY TABLE

Adiabatic Quantum Computers (AQC) are indeed capable of solving Quadratic Mixed Integer Programming (MLIP) problems. This is because these problems can be formulated as Quadratic Unconstrained Binary Optimization (QUBO) problems, which are well-suited for AQCs.

For example, in the field of machine learning, AQCs have been utilized to train models such as Support Vector Machines (SVMs) [14]. The training process, which involves

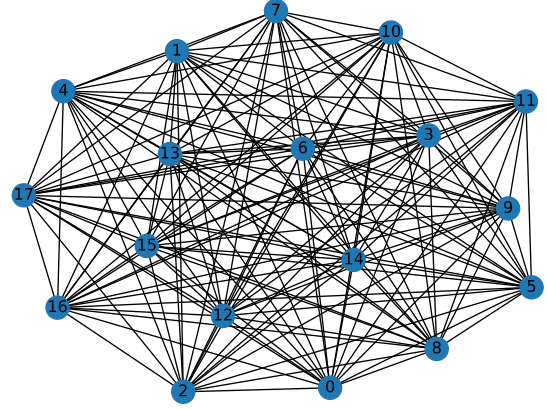


Fig. 17. 18 node input graph

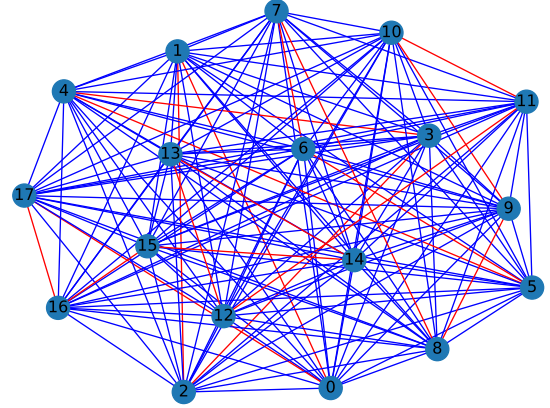


Fig. 18. 18 node output graph

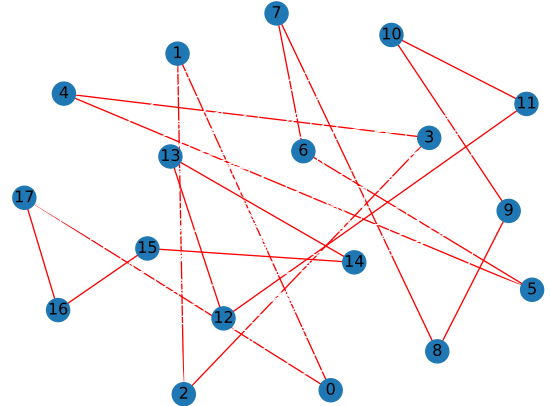


Fig. 19. 18 node output graph with the highlighted solution path

Fig. 20. The 18 node graph solved by QCI Dirac quantum annealers. Plot (a) is the problem graph and plot (b) is the solution graph, Plot (c) is the solution path in the graph

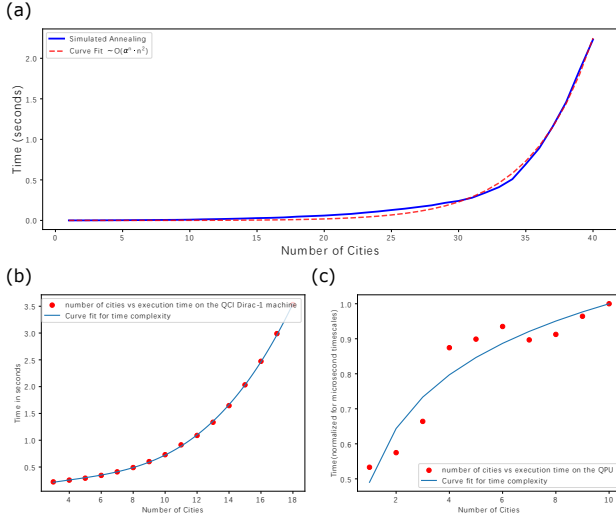


Fig. 21. This is a plot of the algorithm run time for (a) Simulated annealing for TSP instances of sizes upto 40 (b) QCI-Dirac1 for TSP instances of sizes upto 18 (c) D-wave Advantage4.1 for TSP instances of sizes upto 10

solving an optimization problem, can be reformulated as a QUBO problem and effectively tackled using an AQC [15]. In particular, the time complexity of this quantum approach has been demonstrated to be an order of magnitude better than that of classical methods [16].

Furthermore, empirical studies have shown that the quantum approach achieves a 3.5–4.5 times speedup over classical methods when applied to datasets containing millions of features. This indicates that AQCs have the potential to provide substantial advantages in solving Quadratic MLIP problems, particularly for large-scale datasets [21] [9].

Additionally, researchers have demonstrated a quantum speedup for the Traveling Salesman Problem (TSP) on bounded-degree graphs. Specifically, the improvement in computational speed has been shown to be quadratic when the degree of each vertex is at most three [8].

V. CONCLUSION

The time complexities for Ising-type processors are rough estimates based on the curve fitting method, as shown in Figure 21. A more rigorous benchmarking approach is required for improved accuracy in determining time complexity, particularly as constraint violation probability increases with problem size.

Table III presents a comparison between different approaches. It is evident that Ising-type processors provide a definitive speedup for solving specific classes of problems compared to traditional classical computing architectures.

We have demonstrated TSP instances being solved using novel optical, optoelectronic, and quantum hardware and conducted benchmarks to assess the performance limits of currently available commercial machines based on these architectures. NISQ-era universal gate-based quantum

computers, which utilize QAOA and QPE, currently struggle to solve TSP instances exceeding six nodes and rely on classical optimization to determine optimal solutions in the case of QAOA. Quantum annealers have successfully solved TSP instances of up to ten nodes with near-optimal solutions. Meanwhile, optoelectronic Ising machines have demonstrated the ability to handle up to eighteen nodes reliably, although solutions tend to be suboptimal for larger instances. As these technologies continue to evolve, we anticipate that increasingly complex TSP instances will become solvable with greater efficiency and accuracy.

ACKNOWLEDGEMENT

This work was supported in part by the ACC-New Jersey under Contract No. W15QKN-24-C-0004.

REFERENCES

- [1] V. Padmasola and R. Chatterjee, *Optimization on Large Interconnected Graphs and Networks Using Adiabatic Quantum Computation*, International Journal of Quantum Information, vol. 21, no. 6, 2350026, 2023.
- [2] L. Zhou, S.-T. Wang, S. Choi, H. Pichler, and M. D. Lukin, *Quantum Approximate Optimization Algorithm: Performance, Mechanism, and Implementation on Near-Term Devices*, Physical Review X, vol. 10, no. 2, p. 021067, 2020.
- [3] A. M. Dalzell, A. W. Harrow, D. E. Koh, and R. L. La Placa, *How Many Qubits Are Needed for Quantum Computational Supremacy?*, Quantum, vol. 4, p. 264, 2020.
- [4] T. Huang, J. Xu, T. Luo, X. Gu, R. S. M. Goh, and W.-F. Wong, *Benchmarking Quantum(-Inspired) Annealing Hardware on Practical Use Cases*, IEEE Transactions on Computers, vol. 72, no. 6, pp. 1514–1525, 2023.
- [5] E. Stogiannos, C. Paplitis, and T. Andronikos, *Experimental Analysis of Quantum Annealers and Hybrid Solvers Using Benchmark Optimization Problems*, Mathematics, vol. 10, no. 8, p. 1294, 2022.
- [6] S. Jain, *Solving the Traveling Salesman Problem on the D-Wave Quantum Computer*, Frontiers in Physics, vol. 8, p. 760783, 2021.
- [7] T. Zhang and J. Han, *Efficient Traveling Salesman Problem Solvers Using the Ising Model with Simulated Bifurcation*, Proceedings of the Design, Automation & Test in Europe Conference & Exhibition, pp. 1234–1239, 2022.
- [8] A. E. Moylett, N. Linden, and A. Montanaro, *Quantum Speedup of the Traveling-Salesman Problem for Bounded-Degree Graphs*, Physical Review A, vol. 95, no. 3, p. 032323, 2017.
- [9] H. Wang, Y. Pan, and W. Cui, *Quantum-Inspired Solvers on Mixed-Integer Linear Programming Problems*, IEEE Transactions on Computers, vol. 72, no. 4, pp. 1234–1245, 2022.
- [10] K. Srinivasan, S. Satyajit, B. K. Behera, and P. K. Panigrahi, *Efficient Quantum Algorithm for Solving Traveling Salesman Problem: An IBM Quantum Experience*, Quantum Information Processing, vol. 17, no. 8, p. 205, 2018.
- [11] M. Caserta and S. Voß, *A Hybrid Algorithm for the DNA Sequencing Problem*, Discrete Applied Mathematics, vol. 163, pp. 87–99, 2014.
- [12] S. Bock, S. Bommsdorf, N. Boysen, and M. Schneider, *A Survey on the Traveling Salesman Problem and Its Variants in a Warehousing Context*, European Journal of Operational Research, vol. 302, no. 1, pp. 1–16, 2024.
- [13] K. Hoffman and M. Padberg, *Solving Airline Crew Scheduling Problems by Branch-and-Cut*, Management Science, vol. 39, no. 6, pp. 657–682, 1993.
- [14] P. Date, D. J. Woun, K. Hamilton, E. A. Coello Perez, M. C. Shekhar, F. Rios, J. Gounley, I.-S. Suh, T. Humble, and G. Tourassi, *Adiabatic Quantum Support Vector Machines*, in *Proceedings of the 2023 IEEE International Conference on Quantum Computing and Engineering (QCE)*, Bellevue, WA, USA, Sep. 2023, pp. 296–297.
- [15] P. Date and T. Potok, *Adiabatic Quantum Linear Regression*, Scientific Reports, vol. 11, no. 1, p. 21905, Nov. 2021.

- [16] H. R. Wang and L.-A. Wu, *Ultrafast Adiabatic Quantum Algorithm for the NP-Complete Exact Cover Problem*, *Scientific Reports*, vol. 6, p. 22307, Mar. 2016.
- [17] V. Akshay, H. Philathong, M. E. S. Morales, and J. Biamonte, *Reachability Deficits in Quantum Approximate Optimization*, *Physical Review Letters*, vol. 124, no. 9, p. 090504, Mar. 2020.
- [18] T. Bennett, E. Matwiejew, S. Marsh, and J. B. Wang, *Quantum Walk-Based Vehicle Routing Optimisation*, *Quantum Information Processing*, vol. 20, no. 9, p. 295, 2021.
- [19] J. Si, S. Yang, Y. Cen, J. Chen, Z. Yao, D.-J. Kim, K. Cai, J. Yoo, X. Fong, and H. Yang, *Energy-Efficient Superparamagnetic Ising Machine and Its Application to Traveling Salesman Problems*, *Nature Communications*, vol. 14, p. 4501, 2023.
- [20] J. Lamers and G. Verschaffelt, *How to Boost Ising Machines' Ability to Find Optimum Solutions: A Bifurcation Analysis*, in *Proceedings of the 2023 IEEE Photonics Society Summer Topical Meeting Series*, Vancouver, BC, Canada, Jul. 2023, pp. 1–2.
- [21] A. Sannia, A. Giordano, N. Lo Gullo, C. Mastroianni, and F. Plastina, *A Hybrid Classical-Quantum Approach to Speed-Up Q-Learning*, *Scientific Reports*, vol. 13, no. 1, p. 30990, Dec. 2023.
- [22] V. Gilbert, J. Rodriguez, and S. Louise, *Benchmarking Quantum Annealers with Near-Optimal Minor-Embedded Instances*, *Quantum Science and Technology*, vol. 9, no. 2, p. 025001, 2024.
- [23] Y. Kim, A. Eddins, S. Anand, K. Wei, E. Berg, S. Rosenblatt, H. Nayfeh, Y. Wu, M. Zaletel, K. Temme, and A. Kandala, *Evidence for the Utility of Quantum Computing Before Fault Tolerance*, *Nature*, vol. 618, no. 7965, pp. 500–505, Jun. 2023.
- [24] Y. Suzuki, S. Endo, K. Fujii, and Y. Tokunaga, *Quantum Error Mitigation as a Universal Error Reduction Technique: Applications from the NISQ to the Fault-Tolerant Quantum Computing Eras*, *PRX Quantum*, vol. 3, no. 1, p. 010345, Mar. 2022.
- [25] Y. Fang, J. Huang, and Z. Ruan, *Experimental Observation of Phase Transitions in Spatial Photonic Ising Machine*, *Physical Review Letters*, vol. 127, no. 4, p. 043902, Jul. 2021.
- [26] G. Campuzano, C. Obreque, and M. M. Aguayo, *Accelerating the Miller–Tucker–Zemlin Model for the Asymmetric Traveling Salesman Problem*, *Expert Systems with Applications*, vol. 160, p. 113229, Dec. 2020.
- [27] D. L. Applegate, R. E. Bixby, V. Chvátal, and W. J. Cook, *Implementing the Dantzig–Fulkerson–Johnson Algorithm for Large Traveling Salesman Problems*, *Mathematical Programming*, vol. 97, no. 1–2, pp. 91–153, Jul. 2003.
- [28] M. Willsch, D. Willsch, F. Jin, H. De Raedt, and K. Michielsen, *Real-Time Simulation of Flux Qubits Used for Quantum Annealing*, *Physical Review A*, vol. 101, no. 1, p. 012327, Jan. 2020.
- [29] Z. Li, R. Gan, Z. Chen, Z. Deng, R. Gao, K. Chen, C. Guo, Y. Zhang, L. Liu, S. Yu, and J. Liu, *Scalable On-Chip Optoelectronic Ising Machine Utilizing Thin-Film Lithium Niobate Photonics*, *ACS Photonics*, vol. 11, no. 1, pp. 123–130, Jan. 2024.
- [30] Y. Minato, *Two-Step QAOA: Enhancing Quantum Optimization by Decomposing One-Hot Constraints in QUBO Formulations* *arXiv*, 2408.05383, Aug. 2024.
- [31] P. Date, D. Arthur, L.P. Nazzaro, *QUBO formulations for training machine learning models*, *Scientific Reports*, vol. 11, no. 1, p. 10029, May. 2021.
- [32] N. Matsumoto, Y. Hamakawa, K. Tatsumura, K. Kudxo, *Distance-based clustering using QUBO formulations*, *Scientific Reports*, vol. 12, no. 1, p. 2669, Feb. 2022.
- [33] Nguyen, Lac and Miri, Mohammad-Ali and Rupert, R. Joseph and Dyk, Wesley and Wu, Sam and Vrahoretis, Nick and Huang, Irwin and Begliarbekov, Milan and Chancellor, Nicholas and Chukwu, Uchenna and Mahamuni, Pranav and Martinez-Delgado, Cesar and Haycraft, David and Spear, Carrie and Campanelli, Mark and Huffman, Russell and Sua, Yong Meng and Huang, Yuping, *Entropy Computing: A Paradigm for Optimization in an Open Quantum System* *arXiv*, arXiv:2407.04512 [quant-ph], Dec. 2024.